Inorganic Chemistry

Article

pubs.acs.org/IC

Mixed Ligand $Cu^{II}N_2O_2$ Complexes: Biomimetic Synthesis, Activities in Vitro and Biological Models, Theoretical Calculations

Chen Li,[#,†] Bing Yin,[#,†,‡] Yifan Kang,[†] Ping Liu,*[,†] Liang Chen,[§] Yaoyu Wang,[†] and Jianli Li*[,†]

[†]Ministry of Education Key Laboratory of Synthetic and Natural Functional Molecule Chemistry, College of Chemistry & Materials Science, Northwest University, Xi'an, Shaanxi 710069, P. R. China

[‡]College of Chemistry, Beijing Normal University, Beijing 100875, P. R. China

[§]Wuxi PUHE Biotechnology Co., LTD, Wuxi, Jiangsu 214422, P. R. China

Supporting Information

ABSTRACT: Three new mixed ligand $Cu^{II}N_2O_2$ complexes, namely, $[Cu^{II}(2\text{-A-6-MBT})_2(m\text{-NB})_2]$ (**1**), $[Cu^{II}(2\text{-ABT})_2(m\text{-NB})_2]$ (**2**), and $[Cu^{II}(2\text{-ABT})_2(o\text{-NB})_2]$ (**3**), (2-A-6-MBT = 2-amino-6-methoxybenzothiazole, *m*-NB = *m*-nitrobenzoate, 2-ABT = 2-aminobenzothiazole, and *o*-NB = *o*-nitrobenzoate), have been prepared by the biomimetic synthesis strategy, and their structures were determined by X-ray crystallography studies and spectral methods. These complexes exhibited the effective superoxide dismutase (SOD) activity and catecholase activity. On the basis of the experimental data and computational studies, the structure−activity relationship for these complexes was investigated. The results reveal that electron-accepting abilities of these complexes and coordination geometries have significant effects on the SOD activity and catecholase activity. Then, we found that **1** and **2** exerted potent intracellular antioxidant capacity in the model of H_2O_2-induced oxidative stress based on HeLa cervical cancer cells, which were screened out by the cytotoxicity assays of different kinds of cells. Furthermore, **1**−**3** showed the favorable biocompatibility in two different biological models: *Saccharomyces cerevisiae* and human vascular endothelial cells. These biological experimental data are indicative of the promising application potential of these complexes in biology and pharmacology.

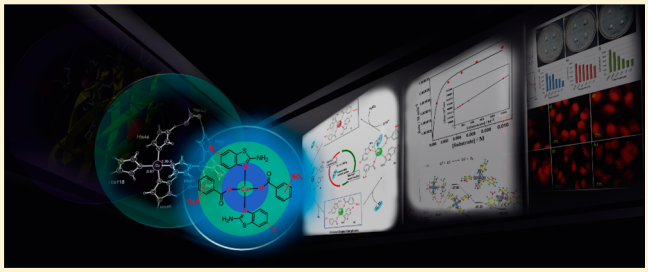

INTRODUCTION

The reactive oxygen species (ROS) is one of the main causes of oxidative stress and contributes to carcinogenesis, atherosclerosis, and Alzheimer's disease.[1] As one of the main ROS in biological systems and a source of other ROS, superoxide radical anion ($O_2^{\bullet-}$) can be catalyzed by superoxide dismutase (SOD) into hydrogen peroxide and dioxygen. Thus, SOD acts as an important antioxidant defense against various pathological conditions that involve cancer, inflammation, cardiovascular diseases, diabetes, ischemia-reperfusion injury, and aging.[2] But as a protein, SOD has several shortcomings in clinical application.[3] To circumvent such limitations, much effort has gone into development of low molecular weight SOD mimics with biological stability, membrane permeability, and nontoxicity.[4] Among the related studies, the $Cu^{II}N_2O_2$ structural motif has received tremendous attention, since it mimics the active site structure of Cu, ZnSOD (Figure 1a), and the complexes with this structural motif ($Cu^{II}N_2O_2$ complexes) exert potent SOD activity.[5] Furthermore, the Cu−N structural fragment is common in the active site of copper-containing enzymes. And for the catechol oxidase, its catalytic activity is based on the Cu−N structural fragment, and thus the complexes with this structural fragment should exhibit the catecholase activity. As expected, such studies have been reported.[6] Given that the $Cu^{II}N_2O_2$ complexes possess a Cu−N structural fragment, it is of great necessity to investigate their catecholase activity.

Although many potent $Cu^{II}N_2O_2$ enzyme mimics have been prepared, two important disadvantages exist in this research field: (1) The structure−activity relationship analysis of these mimics is relatively less,[5d] while the investigation of the structure−activity relationship plays an important guiding role in the studies of enzyme mimics.[7] For facilitating the research, we can divide the complex structure into two parts: the complex inner sphere and complex outer sphere. The complex inner sphere incorporates the central metal and coordination atoms, and the other parts of complex belong to the complex outer sphere. Recently, the influence of outer sphere substituents on the SOD activity of ZnN_4 complexes has been reported,[8] and this study suggests that the outer sphere substituents may have a crucial remote regulation on functional properties of complexes. Thus, it is very necessary to investigate the remote regulation of outer sphere substituents on activities of other enzyme-mimetic complexes. And, as far as we know, the example involving effects of complex outer sphere substituents on activities of $Cu^{II}N_2O_2$ mimics has not yet been reported. (2) Studies of $Cu^{II}N_2O_2$ mimics usually stagnate

Received: September 5, 2014
Published: December 3, 2014

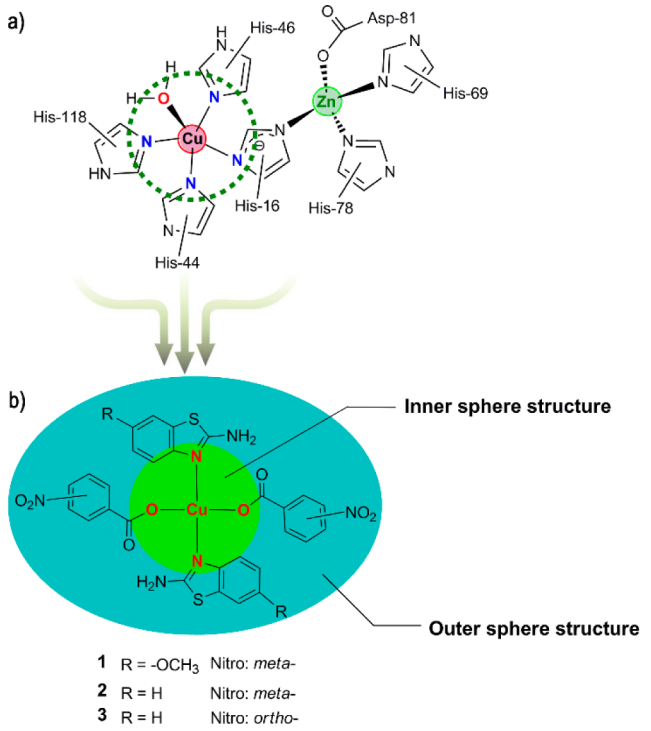

Figure 1. Synthesis of complexes **1**−**3** is based on the active site structure of Cu, ZnSOD. (a) The structure of Cu, ZnSOD. (b) Proposed structures of the complexes **1**−**3**.

in the assessment of their biological activities in vitro. However, the main research purpose of enzyme mimics is the application in vivo, and there are many differences between complexes' biological activities in vitro and in vivo/cell.[9] Therefore, it is of importance to investigate the performance of complexes in biological models for the evaluation of their enzyme-mimetic properties and application potential in biology and medicine science.

Herein, three new mixed ligand copper(II) complexes, namely, $[Cu^{II}(2\text{-A-6-MBT})_2(m\text{-NB})_2]$ (**1**), $[Cu^{II}(2\text{-ABT})_2(m\text{-NB})_2]$ (**2**), and $[Cu^{II}(2\text{-ABT})_2(o\text{-NB})_2]$ (**3**), (2-A-6-MBT = 2-amino-6-methoxybenzothiazole, *m*-NB = *m*-nitrobenzoate, 2-ABT = 2-aminobenzothiazole, and *o*-NB = *o*-nitrobenzoate), are obtained by the biomimetic synthesis strategy, utilizing the $Cu^{II}N_2O_2$ structural biomotif as their inner sphere structure. These complexes are potent SOD mimics and satisfactory catecholase mimics. By an experimental and computational approach, the remote influences of outer sphere substituents on activities of $Cu^{II}N_2O_2$ mimics were investigated. In addition, we also detail the potent intracellular antioxidant potency and favorable biocompatibility of these complexes.

RESULTS AND DISCUSSION

Synthesis, Characterization and Stability. Complexes **1**−**3** were generated by heating cupric chloride dihydrate with corresponding ligands in an water/acetonitrile mixture (1:1, v/v) for 6 h. The three complexes are characterized by the X-ray crystallography study, IR spectroscopy, elemental analysis, solid/solution state UV−vis spectra, and molar conductivity measurement. The proposed structures of complexes **1**−**3** are shown in Figure 1b.

Complexes **1**−**3** are insoluble in all common solvents except DMSO. On dissolution in DMSO, the d−d transition bands of these complexes display small shifts as compared with the solid state. This result suggests that, compared with the solid-state structure, there is no actual change in solution.[10] Furthermore, the conductivity values for **1**−**3** in DMSO, which are below the

Table 1. Summary of the Crystal Structure, Data Collection, and Refinement for 1−3

complex	1	2	3
empirical formula	$C_{30}H_{24}CuN_6O_{10}S_2$	$C_{28}H_{20}CuN_6O_8\ S_2$	$C_{28}H_{20}CuN_6O_8\ S_2$
formula weight	756.21	696.16	696.16
temperature (K)	296(2)	296(2)	296(2)
wavelength (Å)	0.71073	0.71073	0.71073
crystal system	triclinic	triclinic	orthorhombic
space group	$P\bar{1}$	$P\bar{1}$	*Pbcn*
a (Å)	7.1887(1)	7.3711(1)	21.565(3)
b (Å)	9.6527(1)	9.3327(1)	9.4739(1)
c (Å)	12.1714(2)	11.4296(2)	14.027(2)
α (deg)	100.088(2)	89.498(3)	90
β (deg)	105.844(2)	74.108(2)	90
γ (deg)	96.898(2)	76.736(2)	90
vol $(Å)^3$	787.3(2)	734.81(19)	2865.8(7)
Z	1	1	1
D_{calcd} $(mg{\cdot}m^{-3})$	1.595	1.573	1.614
absorption coefficient (mm^{-1})	0.895	0.947	0.971
F(000)	387	355	1420
θ range (deg)	2.18−25.04	2.83−25.05	1.89−25.05
reflections collected/unique	4030/2766	3645/2556	13201/2533
R_{int}	0.0210	0.0223	0.0265
data/restraints/parameters	2766/0/223	2556/0/206	2533/0/204
goodness-of-fit on F^2	1.054	1.026	1.045
final *R* indices $[I > 2\sigma(I)]$: R_1, wR_2	0.0443, 0.1004	0.0448, 0.1020	0.0251, 0.0700
R indices (all data) R_1, wR_2	0.0592, 0.1083	0.0581, 0.1118	0.0295, 0.0728
largest diff. peak and hole $(e{\cdot}Å^{-3})$	0.429 and −0.320	0.467 and −0.534	0.298 and −0.325

dx.doi.org/10.1021/ic5021548 | *Inorg. Chem.* 2014, 53, 13019−13030

Table 2. Selected Bond Lengths (Å) and Bond Angles (deg) for 1−3[a]

1		2		3	
		Bond Lengths			
Cu(1)−O(2)#1	1.949(2)	Cu(1)−O(2)	1.984(2)	Cu(1)−O(1)#1	1.9543(12)
Cu(1)−O(2)	1.949(2)	Cu(1)−O(2)#1	1.984(2)	Cu(1)−O(1)	1.9543(12)
Cu(1)−N(1)#1	1.992(2)	Cu(1)−N(1)	1.986(3)	Cu(1)−N(1)	2.0253(15)
Cu(1)−N(1)	1.992(2)	Cu(1)−N(1)#1	1.986(3)	Cu(1)−N(1)#1	2.0253(15)
O(2)−C(15)	1.280(4)	O(1)−C(8)	1.245(4)	O(1)−C(8)	1.283(2)
O(3)−C(15)	1.236(4)	O(2)−C(8)	1.275(4)	O(2)−C(8)	1.222(2)
		Bond Angles			
O(2)#1−Cu(1)−O(2)	180.00	O(2)−Cu(1)−O(2)#1	180.00(13)	O(1)#1−Cu(1)−O(1)	147.48(8)
O(2)#1−Cu(1)−N(1)#1	90.85(9)	O(2)−Cu(1)−N(1)#1	89.43(10)	O(1)#1−Cu(1)−N(1)	98.69(6)
O(2)−Cu(1)−N(1)#1	89.15(9)	O(2)#1−Cu(1)−N(1)#1	90.57(10)	O(1)−Cu(1)−N(1)	95.34(5)
O(2)#1−Cu(1)−N(1)	89.15(9)	O(2)−Cu(1)−N(1)	90.57(10)	O(1)#1−Cu(1)−N(1)#1	95.34(5)
O(2)−Cu(1)−N(1)	90.84(9)	O(2)#1−Cu(1)−N(1)	89.43(10)	O(1)−Cu(1)−N(1)#1	98.69(6)
N(1)#1−Cu(1)−N(1)	180.000(1)	N(1)#1−Cu(1)−N(1)	180.00	N(1)−Cu(1)−N(1)#1	128.31(9)

[a]Symmetry transformations used to generate equivalent atoms: for **1**: #1 $-x+2, -y+1, -z+1$; for **2**: #1 $-2, -y, -z$; for **3**: #1 $-x+1, y, -z+1/2$.

range of the 1:1 electrolytes (50−70 S cm^2 mol^{-1}), also indicate that there is no significant dissociation when these complexes are dissolved in DMSO.[11]

IR spectra of the three complexes have a similar pattern. The bands corresponding to stretching vibrations of the thiazole rings are observed at 1478.17 (**1**), 1456.70 (**2**), and 1457.60 cm^{-1} (**3**), respectively.[12] In addition, bands that are characteristic of the coordinated carboxylate groups are also found in IR spectra of **1** ($\nu_{asym-OCO}$, 1629.62 cm^{-1}; $\nu_{sym-OCO}$, 1388.01 cm^{-1}), **2** ($\nu_{asym-OCO}$, 1626.53 cm^{-1}; $\nu_{sym-OCO}$, 1396.37 cm^{-1}), and **3** ($\nu_{asym-OCO}$, 1637.94 cm^{-1}; $\nu_{sym-OCO}$, 1348.64 cm^{-1}), respectively.[13] The Δ_{OCO} values of 241.61 cm^{-1} (**1**), 230.16 cm^{-1} (**2**), and 289.3 cm^{-1} (**3**) show that carboxylate groups are coordinated in the monodentate mode.[14]

The structures of **1**−**3** are also determined by X-ray crystallography analysis. Crystallographic data are summarized in Table 1, and Table 2 shows the selected bond distances and bond angles. The results indicate that all complexes **1**−**3** are mononuclear complex. Both **1** and **2** crystallize in the space group $P\bar{1}$, while **3** crystallizes in the *Pbcn* space group. The asymmetric unit of **1** consists of two 2-A-6-MBT molecules, two *m*-NB ligands, and one Cu atom. Each Cu(II) center in complex **1** is four-coordinated by two heterocyclic nitrogen atoms from two 2-A-6-MBT molecules, and two carboxylic oxygen atoms from two *m*-NB ligands, leading to the square planar environment (tetrahedrality = 0°; cf. the tetrahedrality values for idealized geometries are tetrahedrality = 0°, square planar; tetrahedrality = 90°, tetrahedral).[15] Complex **2** is similar to **1**, except that the two coordinated nitrogen atoms from two 2-A-6-MBT molecules are replaced by ones from two 2-ABT molecules. In both **1** and **2**, the O−Cu−N bond angles are nearly 90° (range from 89.15(9)° to 90.85(9)° for **1**, and from 89.43(1)° to 90.57(1)° for **2** respectively), and the N−Cu−N/O−Cu−O bond angles are 180°. All bond lengths and the bond angles are comparable to previously reported works.[4e,5c]

The complex **3** is similar to **2**, except for *ortho*-nitrobenzoate ligands instead of *meta*-position. However, not only the space group but also the bond angles in **3** are different from those found in **2**. In complex **3**, the N−Cu−O angles range from 95.34(5)° to 98.69(6)°, and the N−Cu−N/O−Cu−O angles are 128.31(9)° and 147.48(8)° respectively. These bond angles are similar to the previously reported values of tetrahedral coordination geometries.[5d] The Cu(II) center is in a distorted tetrahedral coordination geometry (tetrahedrality = 59.72°).

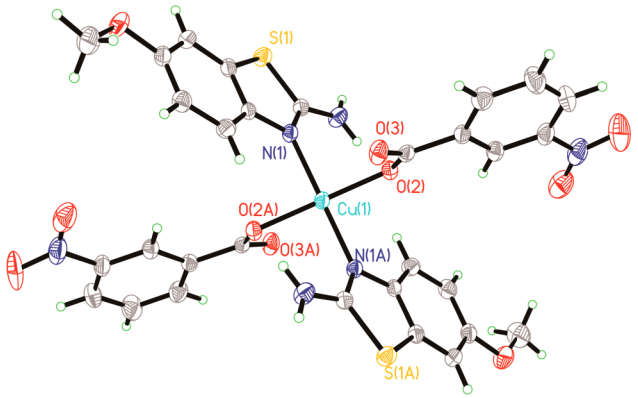

Figure 2. X-ray structure and atom numbering scheme for [Cu^{II}(2-A-6-MBT)$_2$(*m*-NB)$_2$] (**1**).

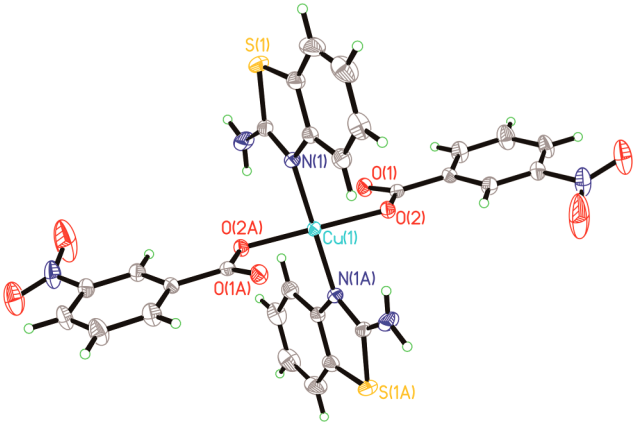

Figure 3. X-ray structure and atom numbering scheme for [Cu^{II}(2-ABT)$_2$(*m*-NB)$_2$] (**2**).

In addition, stability of these complexes in solid state and in DMSO is investigated by thermogravimetric (TG) analyses and UV−vis spectra, respectively. TG analyses indicate that these complexes in the solid state remain stable up to about 200 °C. The time-dependent changes in the UV−vis spectra for these complexes in DMSO over 6 h are shown in Figure 5, and the spectra of **1**−**3** show no noticeable changes. This result shows that these complexes are stable in DMSO solution over 6 h.

dx.doi.org/10.1021/ic5021548 | *Inorg. Chem.* 2014, 53, 13019−13030

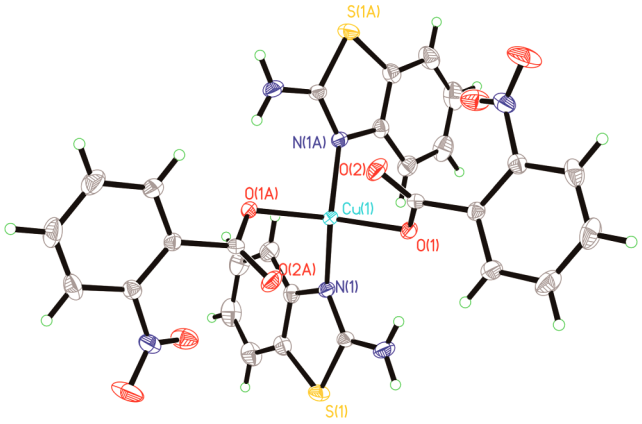

Figure 4. X-ray structure and atom numbering scheme for $[Cu^{II}(2\text{-ABT})_2(o\text{-NB})_2]$ (**3**).

SOD and Catecholase Activity. The SOD activity for **1**−**3** was investigated by an indirect method based on the riboflavin/methionine/nitro blue tetrazolium (NBT) system.[16] Moreover, the activity of Cu, ZnSOD was assayed under the same condition for comparison.

The results (Table 3) show that complexes **1**−**3** all exhibited the effective SOD activity, which is indicative of their application potential as an antioxidant. It is noteworthy that complex **2** is the best SOD mimic among these complexes, and the SOD activity of complex **3** is close to that of **1**.

We also examined the catecholase activities of these complexes, and 3,5-di-*tert*-butylcatechol (3,5-DTBC) was used as the substrate. Before detailed kinetic studies, it is necessary to measure the catecholase activity qualitatively, and 1×10^{-4} M solutions of complexes were treated with 1×10^{-2} M of 3,5-DTBC at 25 °C under aerobic conditions. The reaction system was monitored by UV−vis spectral scans at different times. Complexes **1**−**3** behaved similarly in this reaction with 3,5-DTBC, and a gradual increased peak that corresponds to the product 3,5-DTBQ was observed after adding the complex to the substrate.

Then kinetic reaction experiments of **1**−**3** (at a constant concentration of 1×10^{-4} M) with 3,5-DTBC (varying the concentration from 1×10^{-3} M to 1×10^{-2} M) were performed under aerobic conditions by the UV−vis spectrophotometer. The turnover rates (k_{cat}), which are 16.08 (±0.30) h^{-1} (**1**), 17.63 (±0.08) h^{-1} (**2**), and 9.52 (±0.78) h^{-1} (**3**), suggest that these complexes are moderate catecholase mimics. Complex **2** is also the most effective catecholase mimic among **1**−**3**, and the activity of **3** is much smaller than those of complexes **1** and **2**.

Table 3. SOD Activity Data for Complexes 1−3

complex	$IC_{50}/\mu M$	$k_{cat}/M^{-1}\ s^{-1}$
1	1.21 ± 0.03	$(2.27 \pm 0.06) \times 10^6$
2	1.13 ± 0.04	$(2.42 \pm 0.09) \times 10^6$
3	1.24 ± 0.06	$(2.21 \pm 0.10) \times 10^6$
Cu, ZnSOD[a]	0.0117 ± 0.0024	$(2.40 \pm 0.50) \times 10^8$

[a]The activity of the native Cu, ZnSOD from bovine erythrocytes was assayed under the same condition.

Structure−Activity Relationship Analysis. On the basis of above-mentioned experiment results, it is easy to discover that the SOD activity for these complexes is much better than the catecholase activity. This result may be because the $Cu^{II}N_2O_2$ structural motif is more similar to the active site of Cu, ZnSOD than to the catechol oxidase. Moreover, the Cu−O structural fragment may have a negative impact on the catecholase activity expressed by the Cu−N structural fragment, and this may be another reason for the difference between the SOD activity and catecholase activity. In order to further gain some insight into the structure−activity relationship for these $Cu^{II}N_2O_2$ mimics, these complexes are further investigated by the electrochemical studies and density functional theory (DFT) calculations. The results reveal that these complexes' electron-accepting abilities and coordination geometries, which are influenced by outer sphere substituents, have significant effects on the SOD activity and catecholase activity.

It is reported that the mechanism of SOD activity involves the conversion of $O_2^{\bullet-}$ to O_2, and in this process the Cu(II) center accepts an electron from $O_2^{\bullet-}$.[17] So it is expected that the stronger the electron-accepting ability of copper complex, the more favorable is the electron transfer from $O_2^{\bullet-}$ to Cu(II), and the SOD activity should be better. Similarly, the catecholase activity also involves a process of donating the electron, and the electron is accepted by Cu(II).[18] Therefore, it is supposed that the catecholase activity should be better by increasing the electron-accepting ability of copper complex.

Redox behaviors of **1**−**3** were investigated by the cyclic voltammetry, since it is known that redox properties of complexes are correlated with their catalytic ability. As shown in Table 4, complexes **1**−**3** all exhibited the quasi-reversible one-electron reduction wave, which can be assigned to the Cu^{II}/Cu^{I} pair.[19] The *E* values indicate that their electron-accepting abilities are in the order **2** > **1** > **3**, which is consistent with the catecholase activity variation tendency. And similar to SOD activity, the electron-accepting ability of complex **2** is strongest. Therefore, based on the mechanisms of activities and the favorable relevance between enzyme-mimetic activity data and electrochemical data, it is found that the electron-accepting

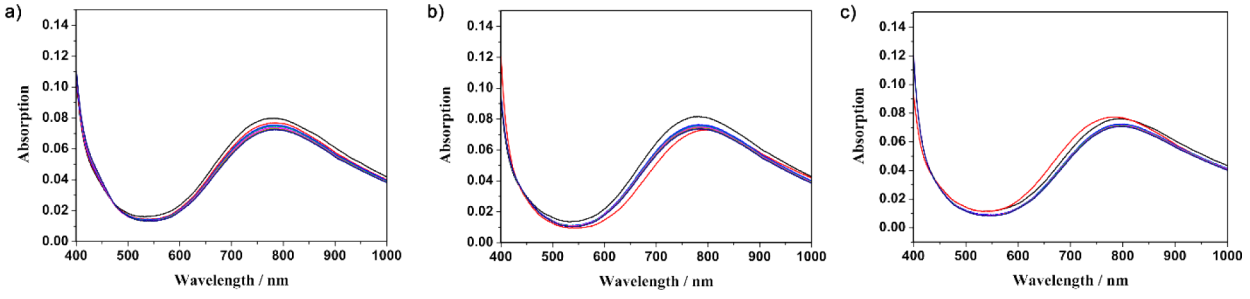

Figure 5. Time-dependent UV−vis spectra for (a) complex **1**, (b) complex **2**, and (c) complex **3** in DMSO; spectra were recorded at *t* = 0 h (black), 1 h (red), 2 h (blue), 3 h (green), 4 h (purple), 5 h (yellow), and 6 h (dark blue) after addition of the complex to DMSO.

dx.doi.org/10.1021/ic5021548 | *Inorg. Chem.* 2014, 53, 13019−13030

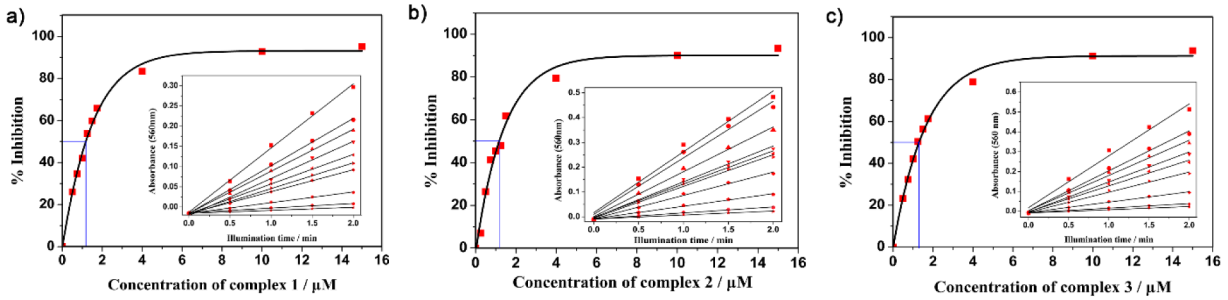

Figure 6. Plots of the percentage of inhibiting NBT reduction with an increase of the concentration for (a) complex **1**, (b) complex **2**, and (c) complex **3**, respectively.

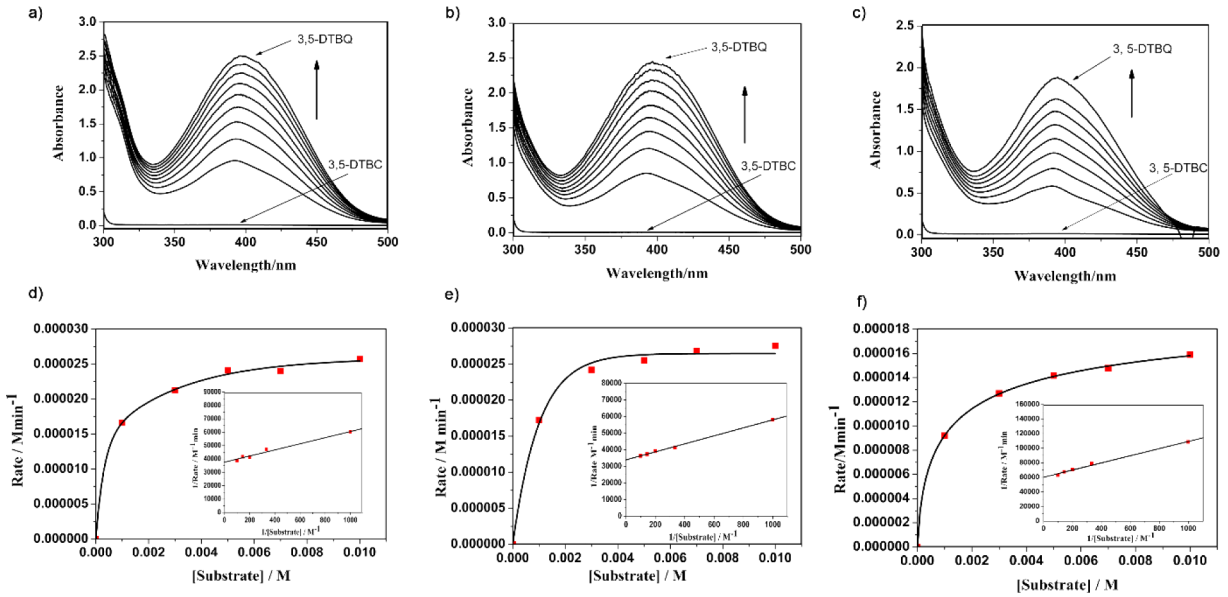

Figure 7. Variations of the spectral behaviors for (a) complex **1** (10^{-4} M), (b) complex **2** (10^{-4} M), and (c) complex **3** (10^{-4} M) in the presence of 3,5-DTBC (10^{-2} M). Plots of rate vs substrate concentration for (d) complex **1**, (e) complex **2**, and (f) complex **3**. Insets show Lineweaver–Burk plots.

Table 4. Cyclic Voltammetric Data for 1–3

complex	E_{pc}/V	E_{pa}/V	E/V[a]	ΔE_p/V[b]
1	−0.916	−0.818	−0.867	0.098
2	−0.786	−0.683	−0.735	0.103
3	−0.994	−0.867	−0.931	0.127

[a]Formal potential E is calculated as $E = (E_{pc} + E_{pa})/2$. [b]$\Delta E_p = E_{pa} - E_{pc}$.

ability has an important influence on the two enzyme-mimetic activities of these complexes.

Furthermore, the differences of coordination geometries also attracted our attention. Accompanied by the outer sphere substituent changes, coordination geometries of **1–3** are varying. Complex **1** and **2** have the same square planar coordination geometry, while complex **3** is distorted tetrahedral coordination geometry, so there exists the larger steric hindrance when the same substrate attack complex **3** as compared to **1** and **2** (Figure 8a).

In addition, DFT calculations were also performed to make a further analysis of two enzyme-mimetic activities of **1–3**. Geometry optimizations and frequency calculations for these complexes and their substrates were performed at the DFT level with B3LYP functional[20] using the Gaussian 09 program package.[21] On the basis of optimized complex structures, the Fukui function $f^+_{(r)}$, which denotes the electron-accepting ability,[22] has been calculated. As shown in Figures 9–11, the spatial distributions of $f^+_{(r)}$ consist of the main contribution from the copper center and its surrounding region, and the values of condensed $f^+_{(r)}$ of copper, based on natural population analysis (NPA),[23] are also significantly larger than those of other atoms. Complex **2** possesses the largest value of condensed $f^+_{(r)}$ of copper, which indicates that this mimic should display the strongest electron-accepting ability, and impressively, the theoretical calculation result is consistent with the above experimental data.

The geometry optimizations of the substrates, which show that the size of $O_2^{\bullet-}$ (1.34 Å) is much smaller than that of 3,5-DTBC (7.31 Å), suggest that the attack of 3,5-DTBC receives the larger steric hindrance than that of $O_2^{\bullet-}$ for the same complex (Figure 8b). Thus, with the change of coordination geometries, the SOD activity of complex **3** is slightly less than those of **1** and **2**, while its catecholase activity is drastically reduced as compared to other complexes. As a result, the coordination geometries have a more significant impact on catecholase activity than that on SOD activity.

In summary, we can obtain the following conclusions: (1) Comparisons of **1** and **2** reveal that methoxy groups on benzothiazole 6 position only affect the electron-accepting ability, while nitro groups of benzoic acid have the influence on

dx.doi.org/10.1021/ic5021548 | Inorg. Chem. 2014, 53, 13019–13030

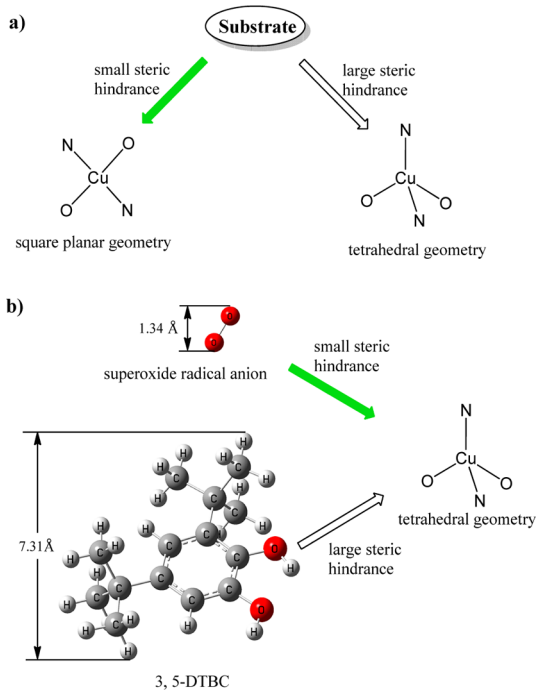

Figure 8. (a) The steric effect caused by coordination geometries. (b) The steric effect caused by the substrate size.

the electron-accepting ability and coordination geometries (**2** vs. **3**). (2) The attack of 3,5-DTBC has a larger steric hindrance than that of $O_2^{\bullet-}$ for the same complex, so the coordination geometries have a more significant effect on the catecholase activity than that on the SOD activity. (3) And complex **2** exerts the most effective reactivity both in two different reactions, for it possesses the strongest electron-accepting ability and square planar coordination geometry. Therefore, the electron-accepting ability and the coordination geometries play important roles in both SOD activity and catecholase activity.

Intracellular Antioxidant Capacity. Complexes **1**−**3** possess the effective antioxidant activity in vitro, and the results have motivated us to investigate their application potential as an intracellular antioxidant. To construct an appropriate cell model assessing the intracellular activity, we examined the cytotoxicity of these complexes on four common kinds of cells including MCF-7 human breast cancer cells, H9C2 rat myocardial cells, HaCat human immortalized epidermal cells, and HeLa cervical cancer cells by the MTT (3-(4,5-dimethyl-2-thiazolyl)-2,5-diphenyltetrazolium bromide) reduction assay.[24] Interestingly, the results show that these complexes promoted cell growth of HaCat human immortalized epidermal cells and HeLa cervical cancer cells with their low concentration, and this suggest that **1**−**3** may alleviate the oxidative damage in the two kinds of cells. According to these results, we chose the cheaper HeLa cervical cancer cells to investigate the intracellular antioxidant activities of **1**−**3**.

To determine an appropriate range of concentration to evaluate the activity of the three complexes in HeLa cells, their cytotoxicity was further evaluated by the MTT assay. In the cytotoxicity assay, cultures of HeLa cells were incubated with 10, 100, or 300 μM complexes for 24 h, respectively. The results reveal that **1** and **3** can promote cell growth with 10 μM and 100 μM, but reduce the cell growth with 300 μM. In contrast, **2** can greatly promote the cell growth with 10 μM,

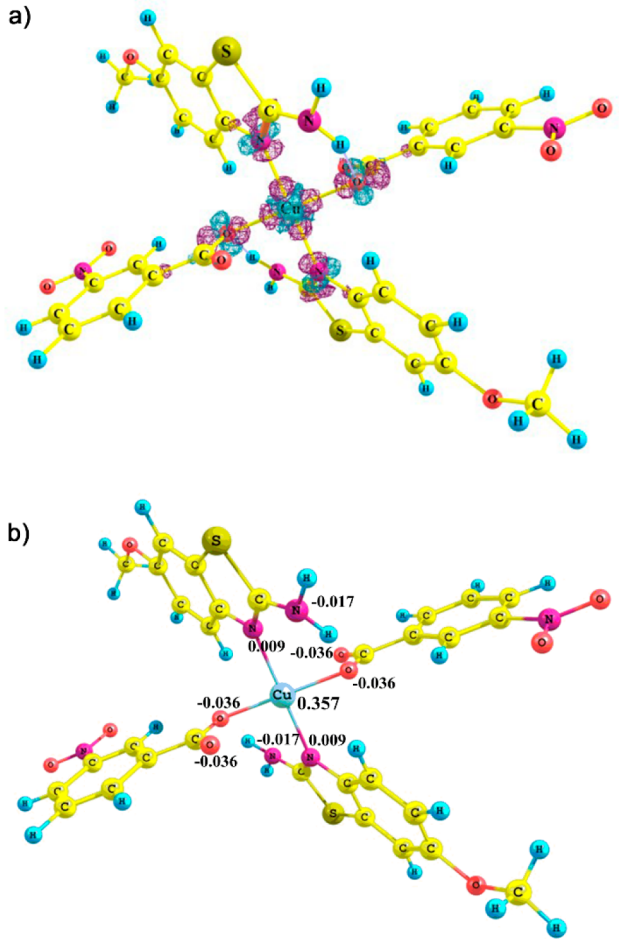

Figure 9. Spatial distribution of Fukui function $f^+_{(r)}$ for complex **1**: (a) The 3D representation of the Fukui function $f^+_{(r)}$ of the isovalue of 0.004 a.u. (positive for red color and negative for green color). (b) The condensed Fukui function $f^+(r)$ of copper and other surrounding atoms.

while the cell growth was restrained with the concentrations of 100 μM and 300 μM.

Then we constructed the model of H_2O_2-induced oxidative stress in HeLa cells to assess the intracellular antioxidant capacity of these complexes. In this model, cellular oxidative damage was studied by examining the ROS distribution using the fluorescence microscopy, which provided an index of the intracellular oxidative metabolism. The ROS distribution revealed the integrity of cell nuclei, and according to the integrity of cell nuclei, we investigated the antioxidant capacity.

As shown in Figure 16, the nuclei displayed good integrity, and no DNA was leaked when cells were directly treated with copper(II) complexes (Figure 16c−e), like the normal HeLa cells (Figure 16b). This result indicates that these complexes have no negative effect on normal HeLa cell growth. In contrast, HeLa cells were severely disrupted by application of H_2O_2-induced oxidative stress, and these HeLa cells served as controls in the study (Figure 16f). In comparison to these controls, the nuclei of HeLa cells, which were pretreated 6 h with H_2O_2, were restored into relatively good integrity when they were exposed to our tested complexes **1** and **2** (Figure 16g,h). These results show that **1** and **2** can alleviate H_2O_2-induced oxidative stress and possess potent intracellular antioxidant capacity. Particularly, **2** exhibited the best protective

dx.doi.org/10.1021/ic5021548 | Inorg. Chem. 2014, 53, 13019−13030

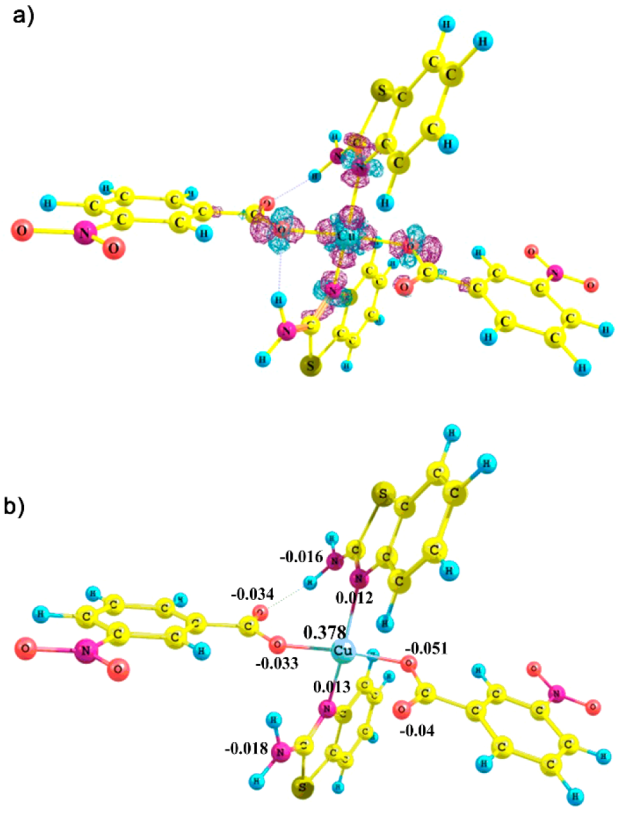

Figure 10. Spatial distribution of Fukui function $f^{+}_{(r)}$ for complex **2**: (a) The 3D representation of the Fukui function $f^{+}_{(r)}$ of the isovalue of 0.004 a.u. (positive for red color and negative for green color). (b) The condensed Fukui function $f^{+}_{(r)}$ of copper and other surrounding atoms.

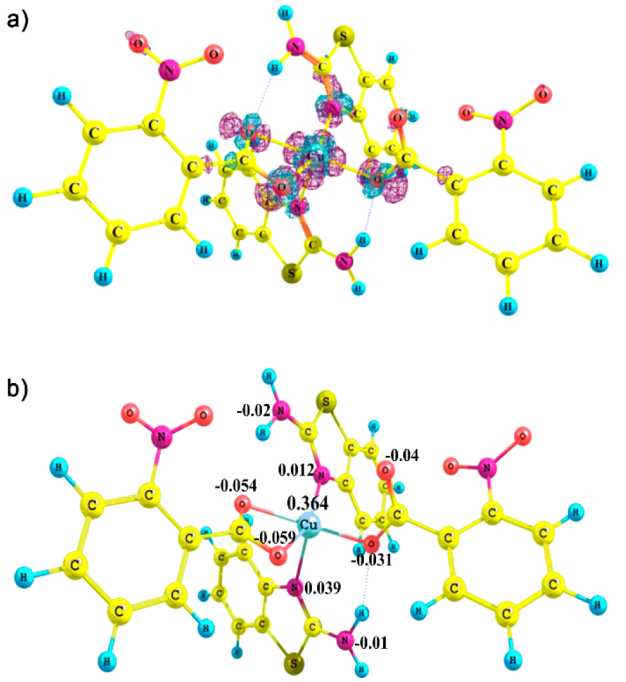

Figure 11. Spatial distribution of Fukui function $f^{+}_{(r)}$ for complex **3**: (a) The 3D representation of the Fukui function $f^{+}_{(r)}$ of the isovalue of 0.004 a.u. (positive for red color and negative for green color). (b) The condensed Fukui function $f^{+}_{(r)}$ of copper and other surrounding atoms.

Table 5. Condensed Fukui Function f^{+} Values of 1−3

atom	1	2	3
Cu	0.357	0.378	0.364
heterocyclic N	0.009	0.012	0.012
heterocyclic N	0.009	0.013	0.039
coordinated carboxylate O	−0.036	−0.033	−0.031
coordinated carboxylate O	−0.036	−0.051	−0.059

role against oxidative damage, and this is consistent with antioxidant activity of complexes in vitro. However, complex **3** had no obvious effect on alleviating ROS production (Figure 16i).

Biocompatibility. For investigating the application potential of **1**−**3** in biology and pharmacology, we examined their biocompatibility in two different biological models: *Saccharomyces cerevisiae* (*S. cerevisiae*) and human vascular endothelial cells (HVECs). The toxicity of **1**−**3** on the *S. cerevisiae* was assessed by the growth inhibition zones caused by these complexes.[25] And no growth inhibition area was observed; this suggest that complexes **1**−**3**, with the tested concentrations, are nontoxic to *S. cerevisiae* (Figure 17). In addition, the cytotoxicity assays of **1**−**3** on HVECs indicate that these complexes have a small cytotoxicity on these cells with low and moderate concentrations (Figure 18).

CONCLUSION

We obtained three new mixed ligand $Cu^{II}N_2O_2$ complexes **1**−**3** by the biomimetic synthesis strategy, and their structures were determined by X-ray crystallography studies and spectral methods. These complexes are the effective SOD mimics and moderate catecholase mimics. The structure−activity relationship for these mimics was analyzed based on the experimental data and DFT calculations. The results reveal that the performances of these complexes in the two enzyme-mimetic activities are affected by their electron-accepting abilities and coordnation geometries. The electron-accepting ability has an important impact on the SOD activity and catecholase activity, and the coordnation geometries have a more significant influence on the catecholase activity than that on the SOD activity due to the different substrate sizes. Moreover, the electron-accepting ability and coordination geometries are changed by varying the outer sphere substituents. Thus, outer sphere substituents have a crucial remote regulation on the functional properties of $Cu^{II}N_2O_2$ complexes. Furthermore, the SOD activity for **1**−**3** is much better than their catecholase activity, and this result may be due to the following two reasons: (1) As compared to catechol oxidase, the $Cu^{II}N_2O_2$ structural motif is more similar to the active site structure of Cu, ZnSOD. (2) The catecholase activity for these complexes may be negatively influenced, which is caused by the Cu−O structural fragment. In addition, the effects of complexes **1**−**3** on the viabilities of different kinds of cells were investigated, and the results revealed that these complexes promoted the cell growth of HaCat human immortalized epidermal cells and HeLa cervical cancer cells with their low concentration. On the basis of these cytotoxicity assays, HeLa cervical cancer cells were screened out to construct the model of H_2O_2-induced oxidative stress, and complexes **1** and **2** exerted potent intracellular antioxidant capacity in this model. Interestingly, the intracellular antioxidant property of complex **2** is best, and this is consistent with the antioxidant activity data in vitro. Futhermore, these complexes show the favorable biocompat-

dx.doi.org/10.1021/ic5021548 | *Inorg. Chem.* 2014, 53, 13019−13030

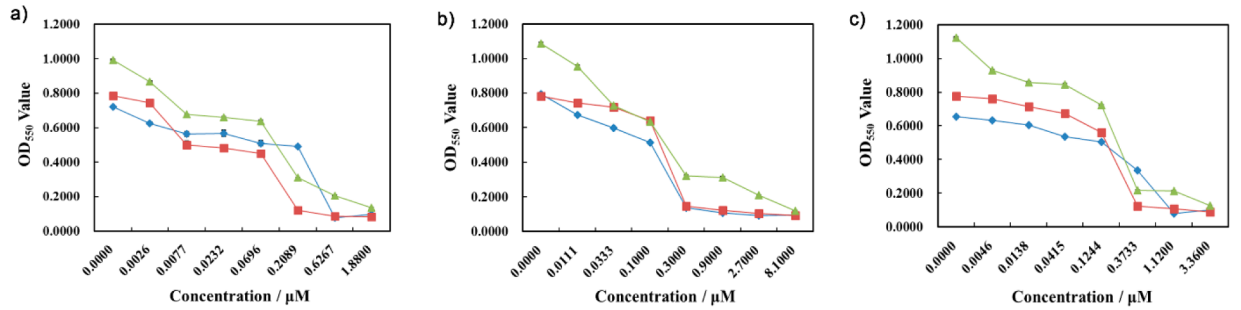

Figure 12. Effects of (a) complex **1**, (b) complex **2**, and (c) complex **3** on the viability of MCF-7 human breast cancer cells for 24 h (blue ◆), 48 h (red ■), and 72 h (green ▲) (MTT assay).

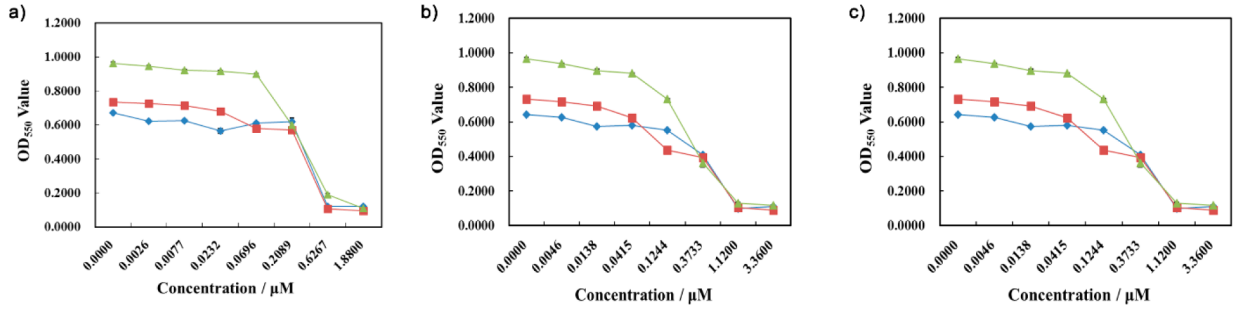

Figure 13. Effects of (a) complex **1**, (b) complex **2**, and (c) complex **3** on the viability of H9C2 rat myocardial cells for 24 h (blue ◆), 48 h (red ■), and 72 h (green ▲)) (MTT assay).

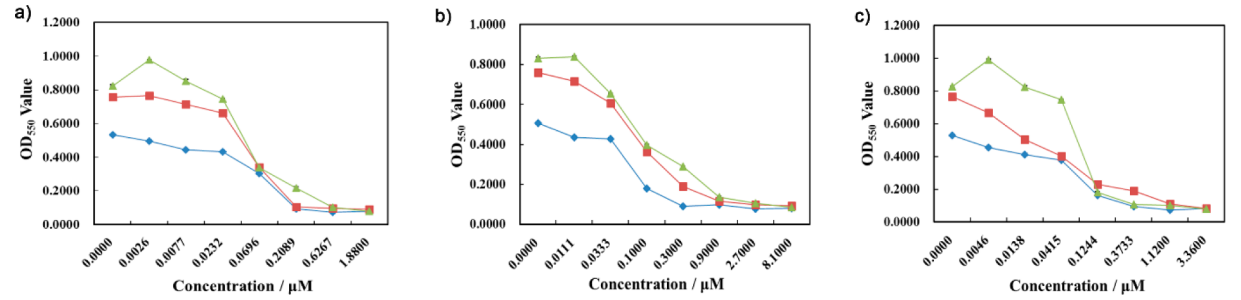

Figure 14. Effects of (a) complex **1**, (b) complex **2**, and (c) complex **3** on the viability of HaCat human immortalized epidermal cells for 24 h (blue ◆), 48 h (red ■), and 72 h (green ▲) (MTT assay).

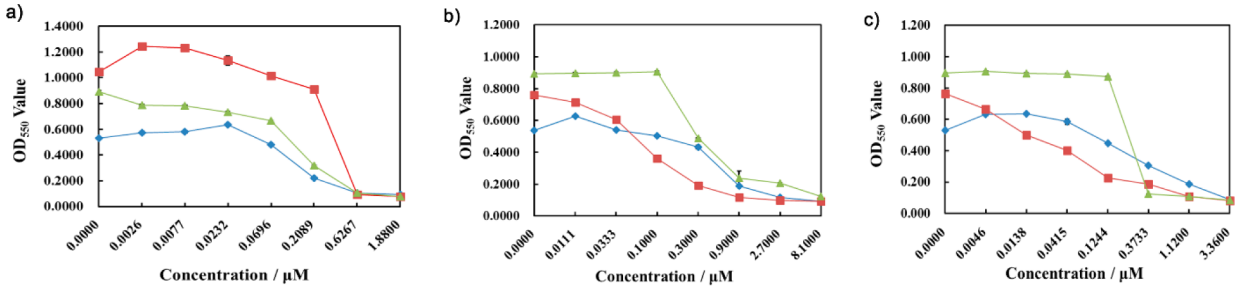

Figure 15. Effects of (a) complex **1**, (b) complex **2**, and (c) complex **3** on the viability of HeLa cervical cancer cells for 24 h (blue ◆), 48 h (red ■), and 72 h (green ▲) (MTT assay).

ibility in *S. cerevisiae* and HVECs. The results obtained in biological models reveal the promising application potential of complexes **1**−**3** in biology and pharmacology.

■ EXPERIMENTAL SECTION

General Procedures. Elemental analyses (C, H, and N) were performed on a Vario EL III Elementar analyzer instrument. Power X-ray diffraction (PXRD) data were recorded using a Rigaku RU200 diffractometer at 60 kV, 300 mA for Cu−Kα radiation (λ = 1.5418 Å), with a scan speed of 2° min^{-1} and a step size of 0.04° in 2 h. IR spectra were recorded with a TENSOR 27 FT-IR Spectrum spectrometer in the region 4000−400 cm^{-1} using KBr pellets. Electronic absorption spectra were recorded by a Shimadzu UV-1700 spectrophotometer in the region 400−1000 nm using cuvettes of 1 cm path length. Diffuse reflectance spectra were registered with a HITACHI U-3310 spectrometer. Thermogravimetric (TG) analyses were performed with a Metter-Toledo TA 50 in dry dinitrogen (60 mL min^{-1}) at a 5

dx.doi.org/10.1021/ic5021548 | *Inorg. Chem.* 2014, 53, 13019−13030

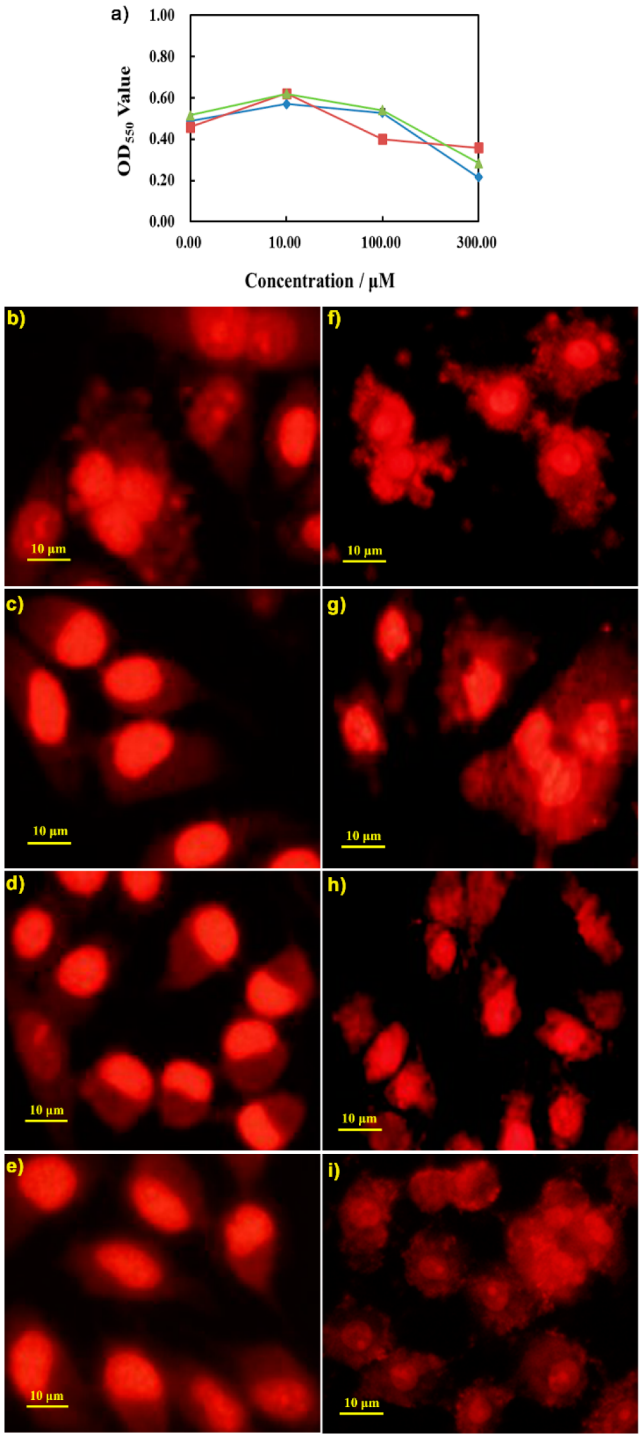

Figure 16. (a) The viabilities of HeLa cervical cancer cells with different concentrations of complex **1** (blue ◆), complex **2** (red ■), and complex **3** (green ▲) for 24 h (MTT assay). The reactive oxygen species (ROS) production images in HeLa cells with different treatments using dihydroethidium (DHE) dye: (b) normal HeLa cells without any treatments, HeLa cells were directly treated with (c) complex **1**, (d) complex **2**, and (e) complex **3**. (f) HeLa cells were exposed to H_2O_2. HeLa cells were preincubated with H_2O_2, followed by adding (g) complex **1**, (h) complex **2**, and (i) complex **3**. The cells were scanned by fluorescence microscopy.

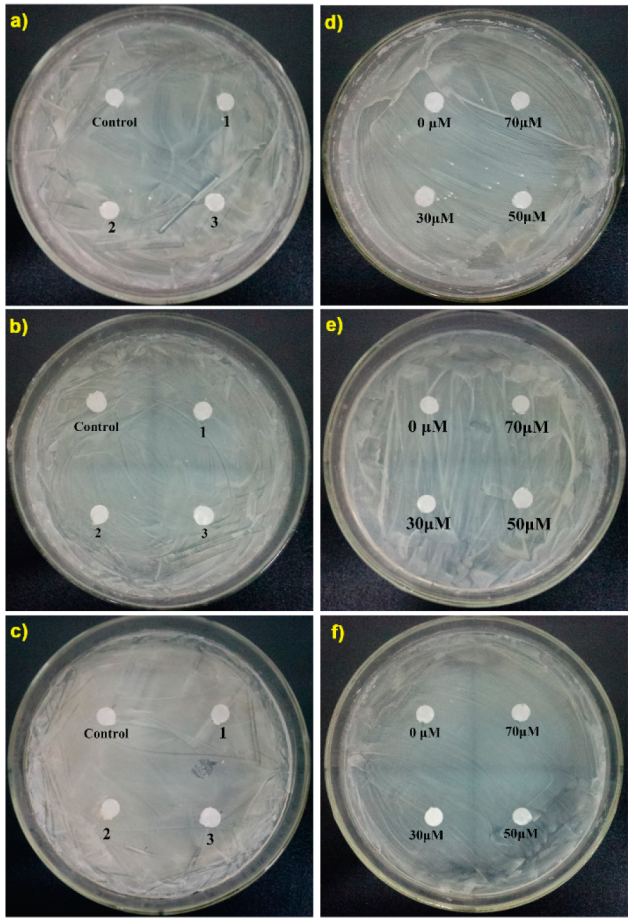

Figure 17. Effects of complexes **1**−**3** on the growth of the *Saccharomyces cerevisiae* with concentrations of (a) 30 μM, (b) 50 μM, and (c) 70 μM. Effects of (d) complex **1**, (e) complex **2**, and (f) complex **3** on the growth of the *S. cerevisiae* with different concentrations (30 μM, 50 μM, and 70 μM, respectively).

°C min^{-1} heating rate. Molar conductivity measurements were made at 20 °C using a DDS-307 conductivity meter.

Synthesis of $[Cu^{II}(2\text{-A-6-MBT})_2(m\text{-NB})_2]$ (1). (2-A-6-MBT = 2-amino-6-methoxybenzothiazole, *m*-NB = *m*-nitrobenzoate). 2-A-6-MBT (360.4 mg, 2 mmol) and *m*-nitrobenzoic acid (334.2 mg, 2 mmol) were dissolved in acetonitrile (40 mL) followed by adding $CuCl_2{\cdot}2H_2O$ (341.0 mg, 2 mmol), and the reaction mixture was heated for 6 h. The resulting solution was left to stand at room temperature. A few days of slow evaporation gave brown red crystals of **1** (591.3 mg, 0.78 mmol), suitable for X-ray diffraction. Yield: 78%. Anal. Calcd (%) for $C_{30}H_{24}CuN_6O_{10}S_2$: C 47.65, H 3.20, N 11.11. Found: C 47.31, H 3.05, N 10.99. IR (KBr), cm^{-1}: 1478.17 (thiazole), 1629.62, 1388.01 (carboxyl); UV−visible in solid state [λ_{max}, nm]: 693. UV−visible (DMSO) [λ_{max}, nm (ε, $M^{-1}cm^{-1}$)]: 767.5 (73.7). Conductivity (DMSO) [Λ_m, S cm^2 mol^{-1}]: 4.23.

Synthesis of $[Cu^{II}(2\text{-ABT})_2(m\text{-NB})_2]$ (2). (2-ABT = 2-aminobenzothiazole). 2-ABT (300.4 mg, 2 mmol) and *m*-nitrobenzoic acid (334.2 mg, 2 mmol) were dissolved in acetonitrile (40 mL) followed by addition of $CuCl_2{\cdot}2H_2O$ (341.0 mg, 2 mmol), and the reaction mixture was heated for 6 h. The resulting solution was left to stand at room temperature. A few days of slow evaporation gave black crystals of **2** (355.4 mg, 0.51 mmol), suitable for X-ray diffraction. Yield: 51% yield. Anal. Calcd (%) for $C_{28}H_{20}CuN_6O_8$: C 48.31, H 2.90, N 12.07. Found: C 48.07, H 2.87, N 11.92. IR (KBr), cm^{-1}: 1456.70 (thiazole), 1626.53, 1396.37 (carboxyl). UV−visible in solid state [λ_{max}, nm]: 726. UV−visible (DMSO) [λ_{max}, nm (ε, M^{-1} cm^{-1})]: 778.0 (86.7). Conductivity (DMSO) [Λ_m, S cm^2 mol^{-1}]: 3.51.

Synthesis of $[Cu^{II}(2\text{-ABT})_2(o\text{-NB})_2]$ (3). (*o*-NB = *o*-nitrobenzoate) 2-ABT(300.4 mg, 2 mmol) and *o*-nitrobenzoic acid (334.2 mg, 2 mmol) were dissolved in acetonitrile (40 mL) followed by addition of $CuCl_2{\cdot}2H_2O$ (341.0 mg, 2 mmol), and the reaction mixture was heated for 6 h. The resulting solution was left to stand at room

dx.doi.org/10.1021/ic5021548 | *Inorg. Chem.* 2014, 53, 13019−13030

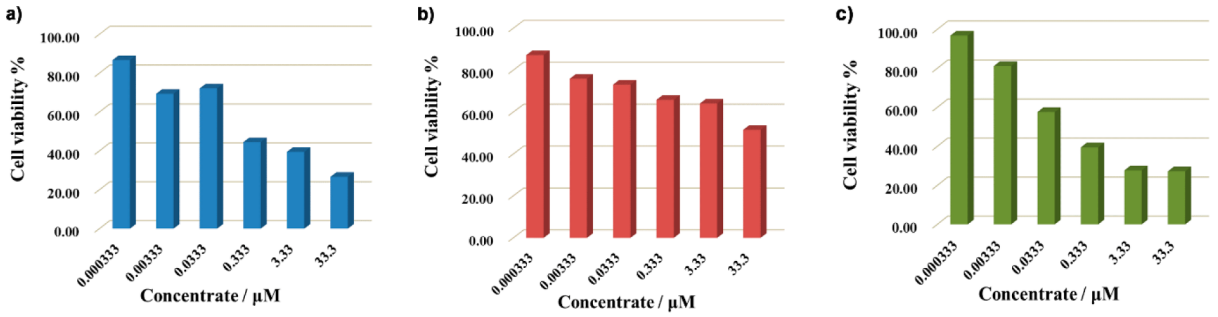

Figure 18. Effects of (a) complex **1**, (b) complex **2**, and (c) complex **3** on the viability of the HVECs.

temperature. A few days of slow evaporation gave black crystals of **3** (334.3 mg, 0.48 mmol), suitable for X-ray diffraction. Yield: 48%. Anal. Calcd (%) for $C_{28}H_{20}CuN_6O_8$: C 48.31, H 2.90, N 12.07. Found: C 48.02, H 2.84, N 11.95. IR (KBr), cm^{-1}: 1457.60 (thiazole), 1637.94, 1348.64 (carboxyl). UV–visible in solid state [λ_{max}, nm]: 846. UV–visible (DMSO) [λ_{max}, nm (ε, M^{-1} cm^{-1})]: 793.5 (77.4). Conductivity (DMSO) [Λ_m, S cm^2 mol^{-1}]: 9.42.

X-ray Crystallography. The single-crystal X-ray data collection was carried out on a Bruker SMART APEX II CCD diffractometer equipped with a graphite monochromated Mo–Kα radiation (λ = 0.71073 Å) at room temperature. Absorption corrections were applied using SADABS.[26] All structures were solved by direct methods and refined by full-matrix least-squares fitting on F^2 by SHELXL-97.[27] The hydrogen atoms of the organic ligands were placed in calculated positions and refined with a riding model.

SOD Activity Experiments. The SOD activity was determined by an indirect method in which the photochemically riboflavin/methionine system was used to generate $O_2^{\bullet-}$. The reaction mixture contained 3.4 μM riboflavin, 46 μM nitro blue tetrazolium (NBT), and 0.01 M methionine in 0.05 M phosphate buffer (pH = 7.8). The reaction system was illuminated by the fluorescent lamp having a constant light intensity at 25 °C. SOD activity was assessed using the IC_{50} value, which represented the concentration of complex yielding 50% inhibition of NBT photoreduction. The IC_{50} value was obtained from a plot of percentage inhibition versus complex concentration. The inhibition percentage was calculated using the following formula:

$$\text{inhibition percentage} = \frac{(k_{\text{without complex}} - k_{\text{complex}})}{k_{\text{without complex}}} \times 100\% \quad (1)$$

The k is the rate of absorbance versus illumination time plot of the reaction system. Moreover, this above assay is on the basis of kinetic competition for $O_2^{\bullet-}$ between NBT and complexes; the reaction rates of NBT and mimics with $O_2^{\bullet-}$ are equal at 50% inhibition, and the catalytic rate constant k_{cat} was obtained by the equation $k_{cat} = k_{NBT}$ [NBT]/IC_{50}, where k_{NBT} = 5.94 × 10^4 M^{-1} s^{-1} is the second-order rate constant for NBT.[28] Moreover, the activity of Cu, ZnSOD was assayed under the same conditions for comparison.

Catecholase Activity Experiments. To investigate the catecholase activity, 3,5-DTBC was used as the substrate. Before detailed kinetic studies, the catecholase activity for **1**–**3** was measured qualitatively. 1 × 10^{-4} M solutions of complexes were treated with 1 × 10^{-2} M of 3,5-DTBC at 25 °C under aerobic conditions. The reaction system was monitored by UV–vis spectral scans at different times (at an interval of 10 min, up to 1.5 h). Kinetic experiments were carried out with the complexes (at a constant concentration of 1 × 10^{-4} M) and 3,5-DTBC (varying the concentration from 1 × 10^{-3} M to 1 × 10^{-2} M) in methanol under aerobic conditions by the UV–vis spectrophotometer. The oxidation of 3,5-DTBC was measured by monitoring the increase in quinone band (quinone band maxima) as a function of time. The dependency of rate on the concentration of substrate was analyzed based on the Michaelis–Menten approach of enzymatic kinetics to obtain the Lineweaver–Burk plot and the values of the kinetic parameters V_{max}, K_M, and k_{cat}.[18,29]

In this reaction, a catalyst–substrate complex (CS) is generated, and then this complex breaks down in the second step to produce the free catalyst (C) and the product (P):

$$C + S \underset{k_2}{\overset{k_1}{\rightleftharpoons}} CS \underset{k_4}{\overset{k_3}{\rightleftharpoons}} C + P \quad (2)$$

The above mechanism results in the well-known Michaelis–Menten equation as shown eq 3a, where V is the rate; [S] represents the concentration of 3,5-DTBC; $K_M = (k_2 + k_3)/k_1$, which is the Michaelis–Menten constant for the mimic; V_{max} represents the maximum rate obtained for a particular concentration of the mimic with a large excess of substrate. The turnover rate $k_{cat} = V_{max}$/[complex], [complex] represents the concentration of complex. By taking the reciprocal of both sides of the Michaelis–Menten equation (eq 3a), the Lineweaver–Burk equation is obtained (eq 3b).

$$V = \frac{V_{max}[S]}{K_M + [S]} \quad (3a)$$

$$\frac{1}{V} = \frac{K_M}{V_{max}} \cdot \frac{1}{[S]} + \frac{1}{V_{max}} \quad (3b)$$

Electrochemistry. Redox potentials of **1**–**3** (0.1 mM) in DMSO with 0.1 M tetra-*n*-butylammonium perchlorate (TBAP) as the supporting electrolyte were measured using the cyclic voltammetry by a CHI 660B electrochemical workstation at room temperature. The conventional three-electrode arrangement was employed. A glassy carbon electrode was used as the working electrode, and a platinum wire was used as the counter electrode. The Ag/AgCl was used as the reference electrode. Experiments were performed at room temperature. Potential was varied from 0 to −1.6 V at a 0.1 V s^{-1} scan rate. Before measurements, oxygen was removed from the solution by bubbling N_2 immediately. Formal potentials were calculated as $E = (E_{pc} + E_{pa})/2$, $\Delta E = E_{pa} - E_{pc}$.

Theoretical Calculation. The DFT calculations were performed with the Gaussian 09 program package using the B3LYP method and basis set of double-ξ quality. The 6-31+G* basis set was used to describe O, N, and S atoms. The DGDZVP[30] basis set was used to describe Cu atom. The 6-31G** basis set was used to describe C and H atoms. The full geometry optimizations for complexes **1**–**3** and substrates were carried out. Vibrational frequency calculations were performed on these optimized structures to ensure the stationary point and no negative frequency was observed.[31] Moreover, the initial geometries were taken from the X-ray crystallography data of **1**–**3** and subjected to optimization. Then the DFT calculations for the Fukui Function $f^+_{(r)}$ were carried out to analyze the activities of complexes. The Fukui function $f^+_{(r)}$ (eq 4a, 4b) represents the ability of accepting the electron.

$$f^+_{(r)} = \left(\frac{\partial \rho(\vec{r})}{\partial N}\right)_\nu = (\rho(\vec{r})_{N+1} - \rho(\vec{r})_N)_\nu \quad (4a)$$

$$f^+_X = q^{N+1}_X - q^N_X \quad (4b)$$

dx.doi.org/10.1021/ic5021548 | Inorg. Chem. 2014, 53, 13019–13030

where $\rho(\vec{r})$ is the electron density, N represents the number of electrons, υ is the external potential, and q_x represents the electronic population of atom X.

Intracellular Antioxidant Capacity Experiments. We investigated the cytotoxicity of these complexes on four common kinds of cells including MCF-7 human breast cancer cells, H9C2 rat myocardial cells, HaCat human immortalized epidermal cells, and HeLa cervical cancer cells by the MTT reduction assay, in order to obtain an appropriate cell model to assess the intracellular antioxidant capacity. The four kinds of cells were all cultured in the complete Dulbecco's modified Eagle's medium (DMEM) and grown at 37 °C in a humidified atmosphere with 5% of CO_2. Then the cell viability was evaluated by the mitochondrial-dependent reduction of MTT to formazan. The cell cultures were incubated without or with different concentrations of complexes for 24, 48, and 72 h, respectively. After that, the cell cultures in 96-well plates were incubated at 37 °C with MTT for 3 h. By aspiration, culture medium was removed, and the cells were solubilized in 0.04 M HCl in absolute ethanol. The reduction of MTT by the cells was quantified by the measuring OD_{550} values. The experiments were performed in triplicate and are presented as the mean of SD.

In order to determine an appropriate range of concentration to evaluate the activity of the three complexes in HeLa cells, we further examined the cytotoxicity of these complexes with different concentrations by the MTT assay. After 24 h of incubation with 0, 10, 100, 300 μM copper(II) complexes, the HeLa cell cultures in the plates were incubated with MTT (0.5 mg/mL) at 37 °C for 3 h.

The model of H_2O_2-induced oxidative stress in HeLa cell was constructed to examine whether these complexes played protective roles against oxidative damage in cells. HeLa cells were preincubated with H_2O_2 (0.5%) for 6 h, followed by adding copper(II) complexes (0.0111 μg/mL) for 24 h, whereas cells were directly treated with copper(II) complexes or H_2O_2 as controls. Dihydroethidium (DHE) is extensively used to monitor ROS production by virtue of its ability to freely permeate cell membranes. DHE reacts with ROS to form the product 2-hydroxyethidium. We examined the distribution of ROS in HeLa cells by DHE. The ROS distribution showed the integrity of cell nuclei. On the basis of the integrity of cell nuclei, we investigated the antioxidant properties of complexes in HeLa cells.

Biocompatibility Experiments. We investigated the toxicity of complexes **1**−**3** on the *S. cerevisiae* by examining the growth inhibition zone caused by these complexes. The *S. cerevisiae* was grown on agar slants at 28 °C for 2 days and inoculated to YPD medium as still cultures at 28 °C for 24 h. Using a Buerkner hemocytometer, yeast concentrations were determined and adjusted to 10^5 per ml. A 200 μL yeast culture liquid was spread on an agar plate. Filter paper disks (diameter = 6 mm) with filter-sterilized samples in different concentrations (30 μM, 50 μM, and 70 μM) were placed on the plates. The plates were incubated in an incubator at 28 °C for 48 h, and the area of the inhibition zone was recorded.

Moreover, the cytotoxicity of complexes **1**−**3** was also evaluated on HVECs. The HVECs line was cultured at 37 °C under a 5% CO_2 atmosphere in RPMI-1640 medium for 24 h. Then the HVECs were extracted and inoculated into the 96-hole cell culture plate for further cell culture. The cell viability was evaluated by the mitochondrial-dependent reduction of MTT. After 24 h of incubation without or with 33.3, 3.33, 0.333, 0.0333, 0.00333, or 0.000333 μM complexes, the HVEC cultures in the 96-hole cell culture plate were incubated with MTT (0.5 mg mL^{-1}) at 37 °C for 1 h. The reduction of MTT by the cells was quantified by the measuring the OD_{550} values.

■ ASSOCIATED CONTENT

Supporting Information

Crystallographic information, theoretical computational details, experimental details. This material is available free of charge via the Internet at http://pubs.acs.org. CIF files for complexes **1**−**3** have been deposited with the Cambridge Crystallographic Data Centre (CCDC 904812, 904814, and 904809, respectively).

■ AUTHOR INFORMATION

Corresponding Authors

*Fax: (+86) 029 88308396. E-mail: lijianli@nwu.edu.cn (J.L.).
*Fax: (+86)029 88302604. E-mail: liuping@nwu.edu.cn (P.L.).

Author Contributions

#C.L. and B.Y. contributed equally to this work.

Notes

The authors declare no competing financial interest.

■ ACKNOWLEDGMENTS

This work was supported by the National Natural Science Foundation of China (NSFC 21272184, 20972124, 21143010, and 21103137), and the Shaanxi Provincial Natural Science Fund Project (No. 2012JQ2007) for financial support. We thank Y. Wang and Y. Huang, Wuxi PUHE Biotechnology Co., LTD., for intracellular antioxidant capacity assays, Dr. Jun Zhang, at the College of Life Science in Northwest University, for toxicity assays on the microorganism, Prof. K.Yan and X. Li, at the National Engineering Research Centre for Miniaturized Detection Systems, for cytotoxicity assays on the somatic cells.

■ REFERENCES

(1) (a) Fukai, T.; Ushio-Fukai, M. *Antioxid. Redox Sign.* **2011**, *15*, 1583−1606. (b) Massaad, C. A.; Washington, T. M.; Pautler, R. G.; Klann, E. *Proc. Natl. Acad. Sci. U.S.A.* **2009**, *106*, 13576−13581. (c) Fukai, T.; Folz, R. J.; Landmesser, U.; Harrison, D. G. *Cardiovasc. Res.* **2002**, *55*, 239−249.

(2) (a) Valko, M.; Leibfritz, D.; Moncol, J.; Cronin, M. T. D.; Mazur, M.; Telser, J. *Int. J. Biochem. Cell B* **2007**, *39*, 44−84. (b) McCord, J. M.; Edeas, M. A. *Biomed. Pharmacother.* **2005**, *59*, 139−142. (c) Church, S. L.; Grant, J. W.; Ridnour, L. A.; Oberley, L. W.; Swanson, P. E.; Meltzer, P. S.; Trent, J. M. *Proc. Natl. Acad. Sci. U.S.A.* **1993**, *90*, 3113−3117.

(3) (a) Salvemini, D.; Muscoli, C.; Riley, D. P.; Cuzzocrea, S. *Pulm. Pharmacol. Ther.* **2002**, *15*, 439−447. (b) Czapski, G.; Goldstein, S. *Free Rad. Res. Commun.* **1991**, *12*−*13*, 167−171.

(4) (a) Gziut, M.; MacGregor, H. J.; Nevell, T. G.; Mason, T.; Laight, D.; Shute, J. K. *Br. J. Pharmacol.* **2013**, *168*, 1165−1181. (b) Rajic, Z.; Tovmasyan, A.; Spasojevic, I.; Sheng, H.; Lu, M.; Li, A. M.; Gralla, E. B.; Warner, D. S.; Benov, L.; Batinic-Haberle, I. *Free Radical Bio. Med.* **2012**, *52*, 1828−1834. (c) Krause, M. E.; Glass, A. M.; Jackson, T. A.; Laurence, J. S. *Inorg. Chem.* **2010**, *49*, 362−364. (d) Potapov, A. S.; Nudnova, E. A.; Domina, G. A.; Kirpotina, L. N.; Quinn, M. T.; Khlebnikov, A. I.; Schepetkin, I. A. *Dalton Trans.* **2009**, 4488−4498. (e) González-Álvarez, M.; Alzuet, G.; Borrás, J.; del Castillo Agudo, L.; García-Granda, S.; Montejo-Bernardo, J. M. *Inorg. Chem.* **2005**, *44*, 9424−9433.

(5) (a) O'Connor, M.; Kellett, A.; McCann, M.; Rosair, G.; McNamara, M.; Howe, O.; Creaven, B. S.; McClean, S.; Kia, A. F.; O'Shea, D.; Devereux, M. *J. Med. Chem.* **2012**, *55*, 1957−1968. (b) Buchtík, R.; Trávníček, Z.; Vančo, J. *J. Inorg. Biochem.* **2012**, *116*, 163−171. (c) Abuhijleh, A. L.; Khalaf, J. *Eur. J. Med. Chem.* **2010**, *45*, 3811−3817. (d) Suksrichavalit, T.; Prachayasittikul, S.; Nantasenamat, C.; Isarankura-Na-Ayudhya, C.; Prachayasittikul, V. *Eur. J. Med. Chem.* **2009**, *44*, 3259−3265.

(6) (a) Agotegaray, M. A.; Dennehy, M.; Boeris, M. A.; Grela, M. A.; Burrow, R. A.; Quinzani, O. V. *Polyhedron* **2012**, *34*, 74−83. (b) Osório, R. E. H. M. B.; Peralta, R. A.; Bortoluzzi, A. J.; de Almeida, V. R.; Szpoganicz, B.; Fischer, F. L.; Terenzi, H.; Mangrich, A. S.; Mantovani, K. M.; Ferreira, D. E. C.; Rocha, W. R.; Haase, W.; Tomkowicz, Z.; Anjos, A. d.; Neves, A. *Inorg. Chem.* **2012**, *51*, 1569−1589.

(7) (a) Okun, Z.; Gross, Z. *Inorg. Chem.* **2012**, *51*, 8083−8090. (b) Reboucas, J. S.; DeFreitas-Silva, G.; Spasojević, I.; Idemori, Y. M.; Benov, L.; Batinić-Haberle, I. *Free Radical Biol. Med.* **2008**, *45*, 201−210. (c) Riley, D. P.; Schall, O. F. *Adv. Inorg. Chem.* **2006**, *59*, 233−

263. (d) Doctrow, S. R.; Huffman, K.; Marcus, C. B.; Tocco, G.; Malfroy, E.; Adinolfi, C. A.; Kruk, H.; Baker, K.; Lazarowych, N.; Mascarenhas, J.; Malfroy, B. *J. Med. Chem.* **2002**, *45*, 4549−4558.
(8) Wada, A.; Jitsukawa, K.; Masuda, H. *Angew. Chem., Int. Ed.* **2013**, *52*, 12293−12297.
(9) (a) Munroe, W.; Kingsley, C.; Durazo, A.; Butler Gralla, E.; Imlay, J. A.; Srinivasan, C.; Selverstone Valentine, J. *J. Inorg. Biochem.* **2007**, *101*, 1875−1882. (b) Riley, D. P. *Chem. Rev.* **1999**, *99*, 2573−2587.
(10) Loganathan, R.; Ramakrishnan, S.; Suresh, E.; Riyasdeen, A.; Akbarsha, M. A.; Palaniandavar, M. *Inorg. Chem.* **2012**, *51*, 5512−5532.
(11) Lu, L.; Yue, J.; Yuan, C.; Zhu, M.; Han, H.; Liu, Z.; Guo, M. *J. Inorg. Biochem.* **2011**, *105*, 1323−1328.
(12) (a) González-Álvarez, M.; Alzuet, G.; Borrás, J.; del Castillo Agudo, L.; García-Granda, S.; Manuel Montejo Bernardo, J. *J. Inorg. Biochem.* **2004**, *98*, 189−198. (b) González-Álvarez, M.; Alzuet, G.; Borrás, J.; Castillo Agudo, L.; Montejo-Bernardo, J. M.; García-Granda, S. *J. Biol. Inorg. Chem.* **2003**, *8*, 112−120.
(13) Devereux, M.; O'Shea, D.; O'Connor, M.; Grehan, H.; Connor, G.; McCann, M.; Rosair, G.; Lyng, F.; Kellett, A.; Walsh, M.; Egan, D.; Thati, B. *Polyhedron* **2007**, *26*, 4073−4084.
(14) Nakamoto, K. *Infrared and Raman Spectra of Inorganic and Coordination Compounds*, 6th ed.; John Wiley & Sons: New York, 2009.
(15) Battaglia, L. P.; Bonamartini Corradi, A.; Marcotrigiano, G.; Menabue, L.; Pellacani, G. C. *Inorg. Chem.* **1979**, *18*, 148−152.
(16) (a) Moreno, D.; Daier, V.; Palopoli, C.; Tuchagues, J. P.; Signorella, S. *J. Inorg. Biochem.* **2010**, *104*, 496−502. (b) Piacham, T.; Ayudhya, C. I. N.; Prachayasittikul, V.; Bülow, L.; Ye, L. *Chem. Commun.* **2003**, 1254−1255. (c) Beauchamp, C.; Fridovich, I. *Anal. Biochem.* **1971**, *44*, 276−287.
(17) Pelmenschikov, V.; Siegbahn, P. E. M. *Inorg. Chem.* **2005**, *44*, 3311−3320.
(18) Banu, K. S.; Chattopadhyay, T.; Banerjee, A.; Mukherjee, M.; Bhattacharya, S.; Patra, G. K.; Zangrando, E.; Das, D. *Dalton Trans.* **2009**, 8755−8764.
(19) Li, Q. X.; Luo, Q. H.; Li, Y. Z.; Shen, M. C. *Dalton Trans.* **2004**, 2329−2335.
(20) (a) Stephens, P. J.; Devlin, F. J.; Chabalowski, C. F.; Frisch, M. J. *J. Phys. Chem.* **1994**, *98*, 11623−11627. (b) Becke, A. D. *J. Chem. Phys.* **1993**, *98*, 5648−5652. (c) Lee, C.; Yang, W.; Parr, R. G. *Phys. Rev. B* **1988**, *37* (2), 785−789.
(21) Frisch, M. J.; Trucks, G. W.; Schlegel, H. B.; Scuseria, G. E.; Robb, M. A.; Cheeseman, R. J.; Scalmani, G.; Barone, V.; Mennucci, B.; Petersson, G. A.; Nakatsuji, H.; Caricato, M.; Li, X.; Hratchian, H. P.; Izmaylov, A. F.; Bloino, J.; Zheng, G.; Sonnenberg, L. J.; Hada, M.; Ehara, M.; Toyota, K.; Fukuda, R.; Hasegawa, J.; Ishida, M.; Nakajima, T.; Honda, Y.; Kitao, O.; Nakai, H.; Vreven, T.; Montgomery, Jr., J. A.; Peralta, J. E.; Ogliaro, F.; Bearpark, M.; Heyd, J. J.; Brothers, E.; Kudin, K. N.; Staroverov, V. N.; Kobayashi, R.; Normand, J.; Raghavachari, K.; Rendell, A.; Burant, C. J.; Iyengar, S. S.; Tomasi, J.; Cossi, M.; Rega, N.; Millam, J. M.; Klene, M.; Knox, J. E.; Cross, J. B.; Bakken, V.; Adamo, C.; Jaramillo, J.; Gomperts, R.; Stratmann, E. R.; Yazyev, O.; Austin, J. A.; Cammi, R.; Pomelli, C.; Ochterski, J. W.; Martin, R. L.; Morokuma, K.; Zakrzewski, V. G.; Voth, G. A.; Salvador, P.; Dannenberg, J. J.; Dapprich, S.; Daniels, A. D.; Farkas, O.; Foresman, J. B.; Ortiz, J. V.; Cioslowski, J.; Fox, D. J. *Gaussian 09*, Revision A.01; Gaussian, Inc.: Wallingford CT, 2009.
(22) (a) Qi, D.; Zhang, L.; Zhao, L.; Cai, X.; Jiang, J. *ChemPhysChem* **2012**, *13*, 2046−2050. (b) Qi, D.; Zhang, L.; Wan, L.; Zhang, Y.; Bian, Y.; Jiang, J. *Phys. Chem. Chem. Phys.* **2011**, *13*, 13277−13286.
(23) Reed, A. E.; Curtiss, L. A.; Weinhold, F. *Chem. Rev.* **1988**, *88*, 899−926.
(24) Bernard, A. S.; Giroud, C.; Vincent Ching, H. Y.; Meunier, A.; Ambike, V.; Amatore, C.; Collignon, M. G.; Lemaître, F.; Policar, C. *Dalton Trans.* **2012**, *41*, 6399−6403.
(25) Wayne, P. *Performance Standards for Antimicrobial Susceptibility Testing*; National Committee for Clinical Laboratory Standards, Wayne, PA, 2001.
(26) Sheldrick, G. M. *SADABS, Empirical Absorption Correction Program*; University of Göttingen: Göttingen: Germany, 1997.
(27) (a) Sheldrick, G. M., *SHELXS-97, Program for X-ray Crystal Structure Solution*; University of Göttingen: Göttingen: Germany, 1997. (b) Sheldrick, G. M., *SHELXL-97, Program for X-ray Crystal Structure Refinement*: University of Göttingen, Göttingen: Germany, 1997.
(28) (a) Durot, S.; Policar, C.; Cisnetti, F.; Lambert, F.; Renault, J. P.; Pelosi, G.; Blain, G.; Korri-Youssoufi, H.; Mahy, J. P. *Eur. J. Inorg. Chem.* **2005**, 3513−3523. (b) Liao, Z. R.; Zheng, X. F.; Luo, B. S.; Shen, L. R.; Li, D. F.; Liu, H. L.; Zhao, W. *Polyhedron* **2001**, *20*, 2813−2821.
(29) Seth, P.; Das, L. K.; Drew, M. G. B.; Ghosh, A. *Eur. J. Inorg. Chem.* **2012**, 2232−2242.
(30) (a) Godbout, N.; Salahub, D. R.; Andzelm, J.; Wimmer, E. *Can. J. Chem.* **1992**, *70*, 560−571. (b) Sosa, C.; Andzelm, J.; Elkin, B. C.; Wimmer, E.; Dobbs, K. D.; Dixon, D. A. *J. Phys. Chem.* **1992**, *96*, 6630−6636.
(31) Foresman, J. B.; Frisch, Æ. *Exploring Chemistry with Electronic Structure Methods*; Gaussian Inc: Pittsburgh PA, 1996.